

Neural Network Equalizers and Successive Interference Cancellation for Bandlimited Channels with a Nonlinearity

Daniel Plabst*, Tobias Prinz*, Francesca Diedolo*, Thomas Wiegart*,
Georg Böcherer†, Norbert Hanik* and Gerhard Kramer*

*School of Computation, Information and Technology, Technical University of Munich, Germany

†Huawei Munich Research Center, Germany

Abstract—Neural networks (NNs) inspired by the forward-backward algorithm (FBA) are used as equalizers for bandlimited channels with a memoryless nonlinearity. The NN-equalizers are combined with successive interference cancellation (SIC) to approach the information rates of joint detection and decoding (JDD) with considerably less complexity than JDD and other existing equalizers. Simulations for short-haul optical fiber links with square-law detection illustrate the gains.

I. INTRODUCTION

Communication systems with hardware constraints or high transmit power may introduce non-linearities, e.g., via a power amplifier (PA) [1] or a square-law detector (SLD) [2]. Non-linearities degrade performance in general, and one may need joint detection and decoding (JDD) to approach capacity. JDD is often too complex [3], and the complexity can be reduced by separate detection and decoding (SDD) for each channel input symbol; see [4], [5]. However, SDD rates may be significantly lower than JDD rates [3], [6]. Two methods that use SDD to approach JDD performance are turbo detection and decoding (TDD) [7]–[9] and multi-level coding (MLC) with successive interference cancellation (SIC) [6], [10]–[12]. TDD requires dedicated code design to approach capacity while MLC-SIC permits using off-the-shelf codes; see [11]–[13].

We consider MLC-SIC, for which one computes a-posteriori probabilities (APPs), e.g., symbol-wise APPs via the forward-backward algorithm (FBA) [14]. Two related methods are (soft-output) Viterbi equalization [15] and Gibbs sampling (GS) [16] to approximate APPs. Linear [3] or non-linear equalizers, such as decision feedback equalizers [17] and Volterra filters [18] may estimate APPs. The main limitation is that, for high rates, either the complexity is high [18], [19] or residual interference reduces rates significantly [3], [6], [19].

We use MLC-SIC with neural network (NN) APP detectors and show one can efficiently achieve high rates for large-memory models. We refer to [20] for a detailed overview of NNs for SDD, JDD and TDD. The literature on MLC-SIC with NNs performs soft-SIC for multiple access [21]–[26] but with no channel decoding between the stages. Thus, significant error propagation may occur if the interference is not entirely suppressed. Also, the information rate is that of SDD.

This paper shows how to approach JDD performance with MLC-SIC and one NN detector per stage. The NN structure is inspired by the FBA, and, in contrast to the NN literature, the receiver decodes between stages and approaches JDD performance as the number of SIC stages increases. To illustrate the gains, we study short-reach fiber links with long memory and an SLD and compare with mismatched SIC equalizers [6]. The NN-SIC receiver outperforms and is substantially simpler than existing receivers that approximate JDD.

This paper is organized as follows. Sec. II introduces the system model with a non-linearity. Sec. III reviews the SDD and SIC rates. Sec. IV describes the NN-APP equalizer. Sec. V presents simulation results, and Sec. VI concludes the paper.

Notation: Column vectors and matrices are written in bold letters, e.g., \mathbf{a} . The transpose of \mathbf{a} is \mathbf{a}^T and $\text{cat}(\mathbf{a}, \mathbf{b}) = [\mathbf{a}^T, \mathbf{b}^T]^T$ stacks \mathbf{a} and \mathbf{b} . The phase of a complex number z is $\angle z$. We denote a string of scalars by $x_\kappa^n = (x_\kappa, \dots, x_n)$ and string of vectors by $\mathbf{X}_\kappa^n = (\mathbf{X}_\kappa, \dots, \mathbf{X}_n)$ and omit the subscript if $\kappa=1$. The sinc function is $\text{sinc}(t) = \sin(\pi t)/(\pi t)$. The convolution of $g(t)$ and $h(t)$ is $g(t) * h(t)$ and the energy of $a(t)$ is $\|a(t)\|^2 = \int_{-\infty}^{+\infty} |a(t)|^2 dt$. Entropy, conditional entropy, and mutual information are defined as in [27, Chap. 2], and we measure the quantities in bits.

II. SYSTEM MODEL

Fig. 1 shows a bandlimited channel with a memoryless non-linear device $\xi(\cdot)$ and additive noise $N'(t)$ after the non-linearity. This model applies to wireless communication with non-linearities at the transmitter due to PAs, mixers, and digital-to-analog converters (DACs), or at the receiver due to low-noise amplifiers (LNAs), mixers, and analog-to-digital converters (ADCs) [1]. The model also describes fiber-optic communications with non-linearities at the transmitter due to a driver amplifier, DAC, modulator, and optical amplifiers, or at the receiver with a square-law detector (SLD), a single photodiode [19], LNA, and ADC. The noise $N'(t)$ might model amplified thermal noise of a radio frequency amplifier [28]–[30], or amplified spontaneous emission noise of an erbium-doped fiber amplifier, or lumped noise of photo-detection [31, Sec. II], the LNA, and the ADC.

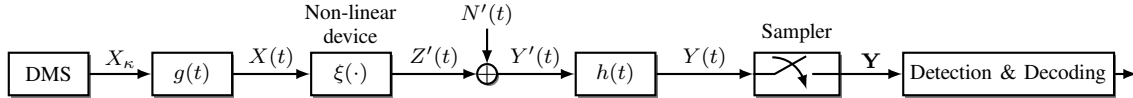


Fig. 1. Bandlimited channel with a memoryless non-linearity and additive noise.

A. Continuous Time Model

A source generates uniformly, independently and identically distributed (u.i.i.d.) symbols $(X_\kappa)_{\kappa \in \mathbb{Z}} = (\dots, X_1, X_2, \dots)$ from the symbol alphabet $\mathcal{A} = \{a_1, \dots, a_M\}$ where $M = 2^m$. After filtering with $g(t)$, the baseband waveform is

$$X(t) = \sum_{\kappa} X_\kappa \cdot g(t - \kappa T_s) \quad (1)$$

where $B = 1/T_s$ is the symbol rate and $g(t)$ collects all linear effects, including the bandwidth limitations of the pulse, non-linear device, and DAC. The non-linear device puts out $Z'(t) = \xi(X(t))$ to which noise $N'(t)$ is added. The noise is modeled as a complex white Gaussian random process with two-sided power spectral density (PSD) $N_0/2$ Watts per Hertz per dimension. The signal and noise are filtered by $h(t)$, which may include a receiver bandwidth limitation and anti-aliasing filter matched to the ADC. Colored noise can be modeled by including a whitening filter in $h(t)$. The filtered noise $N(t) = N'(t) * h(t)$ is a stationary circularly-symmetric complex Gaussian process with autocorrelation function (ACF) $\varphi_{\text{NN}}(\tau) = N_0 \cdot (h^*(-\tau) * h(\tau))$.

B. Memoryless Non-Linear Device

The non-linearity expands the bandwidth, e.g., if $\xi(\cdot)$ is a polynomial of degree d_ξ then $Z'(t)$ occupies d_ξ times the bandwidth of $X(t)$ [32, Sec. 3.1], [33, Thm. 1]. More generally, the bandwidth of $Z'(t)$ may be unbounded but is bandlimited via $h(t)$. To illustrate, consider two applications.

1) *Wireless Transmitter with a PA*: Consider [34] where

$$Z'(t) = \xi(|X(t)|) \cdot \exp(j\angle X(t)) \quad (2)$$

with a non-linear real-valued function $\xi(\cdot)$ that models a solid-state PA that distorts the magnitude; see [29, Sec. 3.2].

2) *Optical Fiber Receiver with a SLD*: Consider a single polarization and the model from [19, Fig. 2] where $g(t) \propto \text{sinc}(Bt) * g_{\text{SSMF}}(t)$ and $g_{\text{SSMF}}(t)$ is the linear response of a standard single-mode fiber (SSMF). The SLD outputs $\xi(\cdot) = |\cdot|^2$ and the front-end of the ADC is a brickwall filter $h(t) \propto \text{sinc}(2Bt)$ with twice the transmit filter bandwidth.

C. Discrete Time Model

We collect samples $Y_k = Y(kT'_s)$, $k \in \mathbb{Z}$, where $T'_s = 1/(BN_{\text{os}})$ corresponds to sampling at rate BN_{os} with oversampling factor N_{os} . The Nyquist-Shannon sampling theorem is met if $Y(t)$ is bandlimited and N_{os} is sufficiently high. The k^{th} receiver sample may be written as

$$Y_k = Z_k + N_k \quad (3)$$

where

$$Z_k = [h(t) * \xi(X(t))]_{t=kT'_s}, \quad N_k = [h(t) * N'(t)]_{t=kT'_s}.$$

The discrete-time noise N_k is stationary, circularly-symmetric, and complex Gaussian with ACF $\varphi_{\text{NN}}[k] = N_0 \cdot \varphi_{\text{NN}}(kT'_s)$.

We address the bandwidth expansion via oversampled simulations. Let $T_{\text{sim}} = T_s/N_{\text{sim}}$ be the simulation sampling period where N_{sim} is the simulation oversampling factor and $d = N_{\text{sim}}/N_{\text{os}}$ is a positive integer. One can approximate

$$Z_k \approx \sum_{u'} h_{u'} \xi \left(\sum_u g_u X'_{(d-k-u')-u} \right) \quad (4)$$

where $(X'_u)_{u \in \mathbb{Z}} = ((0, \dots, 0, X_\kappa))_{\kappa \in \mathbb{Z}}$ is a N_{sim} -fold up-sampled string, and $g_u = g(uT_{\text{sim}})$, $h_u = h(uT_{\text{sim}})$ are the oversampled filters. The SLD example above has $d_\xi = 2$ and $N_{\text{os}} = N_{\text{sim}} = 2$ results in sufficient statistics, and (4) is an equality. However, if $\xi(\cdot)$ is not a polynomial, N_{sim} must be chosen sufficiently large so that (4) is a good approximation.

To illustrate, assume filters g_u and h_u in (4) with odd lengths K_g and K_h , respectively. Suppose their taps are zero outside the intervals $[-\lfloor K_g/2 \rfloor, \lfloor K_g/2 \rfloor]$ and $[-\lfloor K_h/2 \rfloor, \lfloor K_h/2 \rfloor]$. The filters have symbol memories $\tilde{K}_g = \lfloor (K_g - 1)/N_{\text{sim}} \rfloor$ and $\tilde{K}_h = \lfloor (K_h - 1)/N_{\text{sim}} \rfloor$, and the total system memory is

$$\tilde{K} = \tilde{K}_g + \tilde{K}_h. \quad (5)$$

We transmit blocks with $\lfloor K_g/2 \rfloor + \lfloor K_h/2 \rfloor$ zeros at the beginning and end of each block. We collect n transmit symbols in the vector \mathbf{x} and the corresponding N_{os} channel outputs per transmitted symbol in the vector \mathbf{y} , respectively:

$$\mathbf{x} = [x_1, \dots, x_n]^T \in \mathbb{C}^n, \quad \mathbf{y} = [y_1, \dots, y_{N_{\text{os}}n}]^T \in \mathbb{C}^{N_{\text{os}}n}.$$

III. SDD AND SIC RATES

A. SDD Rates

SDD passes symbol-wise APPs $P_{X_\kappa|\mathbf{Y}}(\cdot|\mathbf{y})$, $\kappa \in \{1, \dots, n\}$ to the decoder for data estimation [6, Sec. III]. A lower bound on the information rate of \mathbf{X} and \mathbf{Y} :

$$I_n(\mathbf{X}; \mathbf{Y}) \geq \frac{1}{n} \left(H(\mathbf{X}) - \sum_{\kappa=1}^n H(X_\kappa|\mathbf{Y}) \right) := I_{n,\text{SDD}} \quad (6)$$

with equality if and only if $X_\kappa - \mathbf{Y} - X^{\kappa-1}$. Define the limits

$$I(\mathcal{X}; \mathcal{Y}) := \lim_{n \rightarrow \infty} I_n(\mathbf{X}; \mathbf{Y}), \quad I_{\text{SDD}} := \lim_{n \rightarrow \infty} I_{n,\text{SDD}} \quad (7)$$

so (6) gives $I_{\text{SDD}} \leq I(\mathcal{X}; \mathcal{Y})$. JDD achieves the rate $I(\mathcal{X}; \mathcal{Y})$, but is usually too complex [35]–[37]. In practice, one is often limited to SDD, but [3, Fig. 7-9] and [6, Fig. 6] show that SDD experiences large rate losses in systems with memory.

B. SIC Rates

We use SIC with S stages and a different forward error control (FEC) code for each stage. To encode, downsample \mathbf{X}

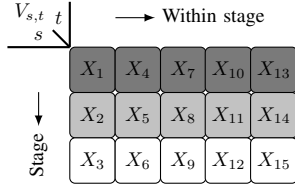


Fig. 2. Encoding with $S = 3$ stages, $N = 5$ and $n = 15$ input symbols.

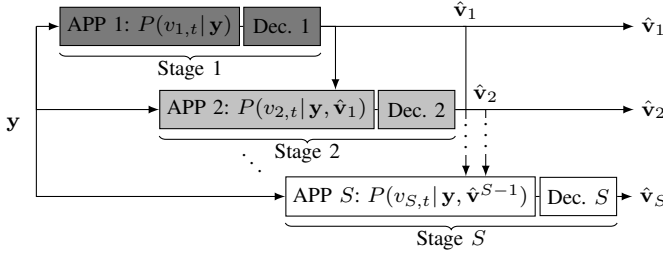


Fig. 3. SIC receiver with SDD for each stage.

by a factor of S to create S sequences of length $N = n/S$; assume N is an integer. The symbols in the s^{th} SIC stage are

$$\mathbf{V}_s = (V_{s,t})_{t=1}^N = (X_{\kappa(s,1)}, X_{\kappa(s,2)} \dots X_{\kappa(s,N)}) \quad (8)$$

where $\kappa(s, t) = s + (t-1)S$ converts a parallel indexing (s, t) to a serial indexing $\kappa(s, t)$. See Fig. 2 as an example with $S = 3$, $n = 15$ and $N = 5$ where $\mathbf{V}_1 = (X_1, X_4, X_7, X_{10}, X_{13})$.

We detect and decode in S stages; see Fig. 3. To illustrate, consider again $S = 3$ and partition \mathbf{X} into $\mathbf{V}_1, \mathbf{V}_2, \mathbf{V}_3$. The first stage performs SDD and calculates APPs for \mathbf{V}_1 . A decoder estimates $\hat{\mathbf{V}}_1$. The second stage uses $\hat{\mathbf{V}}_1$ as prior information and calculates conditional APPs for \mathbf{V}_2 . Correct prior information increases the information rate in the second stage. The final stage calculates APPs for \mathbf{V}_3 , given $(\hat{\mathbf{V}}_1, \hat{\mathbf{V}}_2)$.

Collect $\mathbf{V} = (\mathbf{V}_s)_{s=1}^S$. Since \mathbf{V} is a reordered \mathbf{X} , we have $I_n(\mathbf{X}; \mathbf{Y}) = I_n(\mathbf{V}; \mathbf{Y})$. The average SIC rate is [6, Sec. IV]

$$I_{n,\text{SIC}} = \frac{1}{S} \sum_{s=1}^S I_{N,\text{SIC}}^s \quad (9)$$

with stage rates $I_{N,\text{SIC}}^s := 1/N \sum_{t=1}^N I(V_{s,t}; \mathbf{Y}, \mathbf{V}^{s-1})$ and inequality $I_{n,\text{SDD}} \leq I_{n,\text{SIC}} \leq I_n(\mathbf{V}; \mathbf{Y})$. The limits are $I_{\text{SIC}}^s := \lim_{N \rightarrow \infty} I_{N,\text{SIC}}^s$ and $I_{\text{SIC}} := \lim_{n \rightarrow \infty} I_{n,\text{SIC}}$. We encode \mathbf{V}_s with a code rate less than I_{SIC}^s to ensure reliable decoding as the block length grows, i.e., we may assume $\hat{\mathbf{V}}_s = \mathbf{V}_s$; see [11]. Comparing the limiting rates, we obtain

$$I_{\text{SDD}} \leq I_{\text{SIC}} \leq I(\mathcal{X}; \mathcal{Y}). \quad (10)$$

SIC can approach the JDD performance by increasing S [6, Fig. 6]. Note that SDD has $S = 1$.

IV. NN-APP DETECTOR

Running the FBA in every SIC stage is too complex even for relatively small memory \tilde{K} or alphabets \mathcal{A} , so one must use mismatched models. We propose an NN with an FBA structure that is recurrent and periodically time-varying [20]. Fig. 4 shows the recurrent NN (RNN), which consists of multiple layers. Each layer is bidirectional with a forward and backward path and internal states similar to the FBA [38], [39].

A. NN Structure and Processing

Suppose the NN inputs are real-valued or use composite-real representations for complex-valued inputs. In SIC stage s we process inputs for the remaining $j = s, \dots, S$ stages:

$$\mathbf{r}_{j,t}^1 := (\bar{\mathbf{y}}_{j,t}, \bar{\mathbf{v}}_{j,t}) \in \mathbb{R}^{L_Y + L_{\text{IC}}} \quad (11)$$

with L_Y channel outputs $\bar{\mathbf{y}}_{j,t}$ and L_{IC} symbols $\bar{\mathbf{v}}_{j,t}$. We use

$$\bar{\mathbf{y}}_{j,t} := (y_{N_{\text{os}}, \kappa(j,t)+u})_{u=-\Delta}^{\nabla} \in \mathbb{R}^{L_Y} \quad (12)$$

where $\Delta := \lfloor (L_Y - 1)/2 \rfloor$ and $\nabla := \lceil (L_Y - 1)/2 \rceil$ correspond to symbols before and after transmission of the symbol $v_{j,t} = x_{\kappa(j,t)}$, respectively. Next, collect the L_{IC} symbols among \mathbf{v}^{s-1} that are closest to $v_{j,t} = x_{\kappa(j,t)}$ in the vector

$$\bar{\mathbf{v}}_{j,t} := (x_{\kappa} \mid \kappa \in \mathcal{V}_{j,t}) \in \mathbb{R}^{L_{\text{IC}}} \quad (13)$$

where ‘‘closest’’ means

$$\mathcal{V}_{j,t} = \underset{|\mathcal{U}|=L_{\text{IC}}}{\text{argmin}} \sum_{a \in \mathcal{U}, x_a \in \mathbf{v}^{s-1}} |a - \kappa(j,t)|. \quad (14)$$

We use zero-padding to extend the vectors (12) where needed.

RNN inputs are processed in forward and backward order:

$$\dots \mathbf{r}_{s,t}^1, \mathbf{r}_{s+1,t}^1, \dots, \mathbf{r}_{S,t}^1, \mathbf{r}_{s,t+1}^1, \mathbf{r}_{s+1,t+1}^1, \dots, \mathbf{r}_{S,t+1}^1 \dots \quad (15)$$

and stage s processes a total of $N(S-s+1)$ inputs. The input-process (15) for stages s to S is cyclostationary with period $S-s+1$ due to the SIC partitioning of Sec. III-B. Likewise, the FBA state metrics are cyclostationary [20] with the same period. We thus adapt classic RNNs [40, Chap. 10.3] to periodically time-varying input processing and state recursions.

Fig. 4 shows the structure of such a time-varying RNN with L layers: $L-1$ layers are recurrent with forward and backward paths, and the last layer is feedforward. Consider the forward path in layer i . This path has cells $\tilde{C}_s^i, \tilde{C}_{s+1}^i, \dots, \tilde{C}_S^i$ that repeat periodically for $t = 1, \dots, N$. Compared to classic RNNs [40, Chap. 10.3], the number of RNN parameters increases by a factor of $S-s+1$, but the computational complexity remains the same. RNNs have internal states $(\tilde{\mathbf{h}}_{j,t}^i)_{j=s}^S$ in the forward and backward paths, where $t = 1, \dots, N$.

To illustrate further, let the input dimensions of the recurrent layers and the output layer be $(\ell_1, \dots, \ell_{L-1}, \ell_L)$, where $\ell_1 = L_Y + L_{\text{IC}}$. We convert the pairs (11) to column vectors. The state recursion via cells \tilde{C}_j^i , $j = s, \dots, S$, is

$$\tilde{\mathbf{h}}_{j,t}^i = f(\tilde{\mathbf{W}}_{\text{in},j}^i(\mathbf{r}_{j,t}^i) + \tilde{\mathbf{W}}_{j-1}^i(\tilde{\mathbf{h}}_{j-1,t}^i)) \in \mathbb{R}^{\ell_{i+1}/2} \quad (16)$$

where $f(\cdot)$ is the element-wise rectified linear unit (ReLU), and the index pair $(s-1, t) \mapsto (S, t-1)$ as well as the single index $s-1 \mapsto S$ due to the parallel indexing. The input and state transformations for $j = s, \dots, S$ are:

$$\begin{aligned} \tilde{\mathbf{W}}_{\text{in},j}^i: \mathbb{R}^{\ell_i} &\mapsto \mathbb{R}^{\ell_{i+1}/2}, & \tilde{\mathbf{W}}_{\text{in},j}^i(\mathbf{r}_{j,t}^i) &= \tilde{\mathbf{W}}_{\text{in},j}^i \mathbf{r}_{j,t}^i + \tilde{\mathbf{b}}_{\text{in},j}^i \\ \tilde{\mathbf{W}}_j^i: \mathbb{R}^{\ell_{i+1}/2} &\mapsto \mathbb{R}^{\ell_{i+1}/2}, & \tilde{\mathbf{W}}_j^i(\tilde{\mathbf{h}}_{j,t}^i) &= \tilde{\mathbf{W}}_j^i \tilde{\mathbf{h}}_{j,t}^i + \tilde{\mathbf{b}}_j^i \end{aligned}$$

where $\tilde{\mathbf{W}}_{\text{in},j}^i$, $\tilde{\mathbf{W}}_j^i$ and $\tilde{\mathbf{b}}_{\text{in},j}^i$, $\tilde{\mathbf{b}}_j^i$ are input and state recursion matrices, and input and state bias vectors, respectively. The backward path works analogously; see Fig. 4.

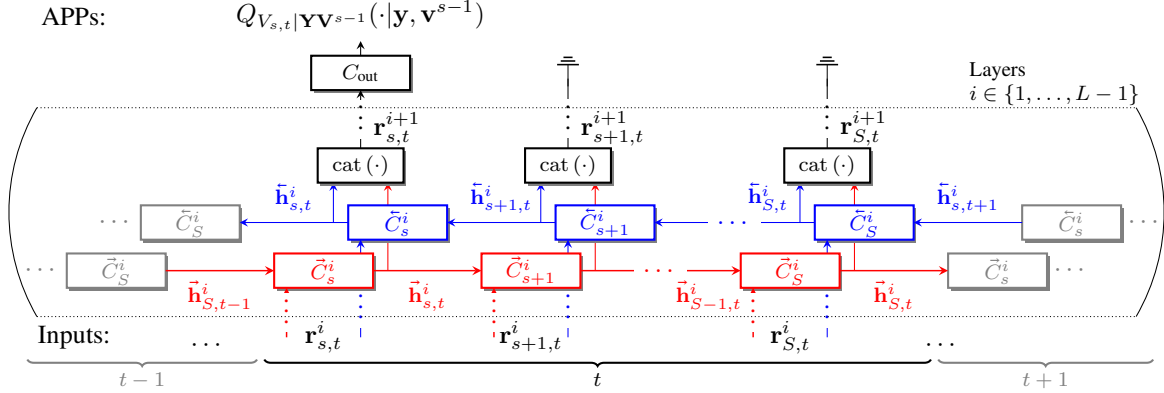


Fig. 4. Bidirectional time-varying RNN for SIC stage s .

To complete the recurrent layer processing, the outputs of the two paths are concatenated for $j = s, \dots, S$ and all t :

$$\mathbf{r}_{j,t}^{i+1} = \text{cat}(\bar{\mathbf{h}}_{j,t}^i, \tilde{\mathbf{h}}_{j,t}^i) \in \mathbb{R}^{\ell_{i+1}} \quad (17)$$

and (17) is passed to the next recurrent layer if $i + 1 < L$. If $i + 1 = L$, the last cell C_{out} performs final processing, i.e., for all t and fixing $j = s$ we have

$$Q_{V_{s,t}|\mathbf{Y}, \mathbf{V}^{s-1}}(\cdot|\mathbf{y}, \mathbf{v}^{s-1}) = \phi(\mathbf{W}_{\text{out}}\mathbf{r}_{s,t}^L + \mathbf{b}_{\text{out}}) \in \mathbb{R}^{|\mathcal{A}|} \quad (18)$$

where $\mathbf{W}_{\text{out}} \in \mathbb{R}^{|\mathcal{A}| \times \ell_L}$, $\mathbf{b}_{\text{out}} \in \mathbb{R}^{|\mathcal{A}|}$, and the ‘‘softmax’’ function $\phi(\cdot)$ [41] generates a PMF interpreted as symbol-wise APPs. To initialize the RNN, we set the first forward and last backward states in all recurrent layers to zero.

B. Achievable Rates and NN Optimization

The NN-APP detector approximates APPs (18). A lower-bound on the SIC rate is (see [6, Sec. VI D.], [42])

$$I_{n,\text{SIC}} \geq \frac{1}{S} \sum_{s=1}^S \frac{1}{N} \sum_{t=1}^N \underbrace{H(V_{s,t}) + \mathbb{E}[\log_2 Q(V_{s,t}|\mathbf{Y}, \mathbf{V}^{s-1})]}_{:= I_{q,N,\text{SIC}}^s}$$

where the expectation is over the actual $p_{V_{s,t}|\mathbf{Y}, \mathbf{V}^{s-1}}$. The expression $I_{q,N,\text{SIC}}^s$ is the mismatched rate of SIC stage s and we define the limiting rate as $I_{q,\text{SIC}}^s := \lim_{N \rightarrow \infty} I_{q,N,\text{SIC}}^s$.

We wish to maximize $I_{q,N,\text{SIC}}^s$ for each SIC stage s . We estimate $I_{q,N,\text{SIC}}^s$ via simulation and formulate the optimization problem as a cross-entropy minimization [43, Sec. 4.1]

$$\underset{(Q_{V_{s,t}|\mathbf{Y}, \mathbf{V}^{s-1}})_{t=1}^N}{\text{argmin}} - \frac{1}{N} \sum_{t=1}^N \langle \log_2 Q_{V_{s,t}|\mathbf{Y}, \mathbf{V}^{s-1}}(v_{s,t}|\mathbf{y}, \mathbf{v}^{s-1}) \rangle \quad (19)$$

where $\langle \cdot \rangle$ denotes Monte-Carlo averaging over N_{blk} transmit symbols and pairs $(\mathbf{v}^{(w)}, \mathbf{y}^{(w)})_{w=1}^{N_{\text{blk}}}$ with the APPs (18).

We optimize one NN per SIC stage and SNR. The NNs are initialized with optimized parameters from a lower SNR, if available. We approximate (19) via ADAM [44] and perform stochastic batch gradient descent with strings $(\mathbf{v}^{(w)}, \mathbf{y}^{(w)})_{w=1}^{N_{\text{batch}}}$ generated each from $N = T_{\text{RNN}}/(S-s+1)$ channel inputs; the parameter T_{RNN} limits the number of sequential RNN inputs to avoid numerical instabilities [45]. We take N_{iter} gradient

TABLE I
ALGORITHMIC COMPLEXITY PER APP ESTIMATE.

Algorithm	Multiplications
FBA [19]	$\mathcal{O}(S \cdot \mathcal{A} ^{\bar{K}+1})$
Bit-wise GS [6]	$\mathcal{O}(S \cdot \bar{K}^2 \cdot m \cdot N_{\text{iter}} \cdot N_{\text{par}})$
NN	$\mathcal{O}(S \cdot (\sum_{i=1}^{L-1} \ell_i \ell_{i+1} + \ell_{i+1}^2/2 + \ell_L \cdot \mathcal{A}))$

steps with step size β_{lr} . The number of inputs T_{RNN} and size L_Y indicate the maximum symbol memory that the RNN can capture and is $\tilde{N}_{\text{RNN}} \approx \lfloor L_Y/N_{\text{os}} \rfloor + (T_{\text{RNN}} - 1)$.

V. NUMERICAL RESULTS

We study detection for short-haul fiber-optic links with a SLD $\xi(\cdot) = |\cdot|^2$, which is a phase-retrieval problem [46]; see Sec. II-B2. The program code is available at [47].

We transmit N_{blk} blocks, each with $n \geq 20 \cdot 10^3$ symbols, and evaluate the SIC rates (19) via Monte Carlo simulation. The DAC performs sinc pulse shaping at the symbol rate 35 GBd. We consider $L_{\text{fib}} = 30$ km of SSMF without fiber attenuation, operated at the C band carrier $\lambda = 1550$ nm. The group velocity dispersion is $\beta_2 = -2.168 \cdot 10^{-23}$ s²/km. The sinc pulse and dispersion introduce long memory in the combined channel $g(t)$. The SLD doubles the signal bandwidth to $2B$. The receiver uses a brickwall filter $h(t)$ with bandwidth $2B$. Oversampling $Y(t)$ with $N_{\text{sim}} = N_{\text{os}} = 2$ provides sufficient statistics. We approximate $g(t)$ by a discrete filter g_k with $K_g = 151N_{\text{sim}} + 1$ taps, with a symbol memory of $\bar{K}_g = 151$. The filtered and sampled noise N_k is real AWGN. The filter $h(t)$ does not impact the receive signal component, and hence the total memory (5) is $\bar{K} = \bar{K}_g$. The average transmit power is $P_{\text{tx}} = 1/(nT_s) \mathbb{E}[\|X(t)\|^2]$ and we choose the noise variance $\sigma^2 = 1$, so $\text{SNR} = P_{\text{tx}}$. The NN parameters are found empirically and are listed in Tab. II. We compare unipolar M -PAM with $\mathcal{A} = \{0, 1, \dots, 2^m - 1\}$ to bipolar M -ASK with $\mathcal{A} = \{\pm 1, \pm 3, \dots, \pm(2^m - 1)\}$; for complex-valued modulation, see [20]. We use differential phase encoding [6] before the DAC to help resolve phase ambiguities. We plot SIC rates in bits per channel use (bpcu) for the mismatched FBA [19], GS [6] and NN detectors. Tab. I compares the

TABLE II
NN PARAMETERS.

Modulation	$L_Y, \ell_2, \ell_3, \ell_4, \ell_5$	\tilde{N}_{RNN}	L_{IC}	T_{RNN}	N_{batch}	N_{blk}	n	β_{Ir}	N_{iter}	L_{fib} [km]
$M = 4$	64, 128, 64	95	32	64	128	$1 \cdot 10^3$	$6 \cdot 10^4$	$5 \cdot 10^{-4}$	$2 \cdot 10^4$	30
$M = 8$	64, 128, 128	115	32	84	128	$1 \cdot 10^3$	$6 \cdot 10^4$	$3 \cdot 10^{-4}$	$5 \cdot 10^4$	30
$M = 16$	84, 200, 128, 128	161	64	120	64	$3 \cdot 10^3$	$8 \cdot 10^4$	$5 \cdot 10^{-5}$	$8 \cdot 10^4$	30
$M = 32$	100, 200, 200, 200, 168	169	64	120	64	$7 \cdot 10^3$	$8 \cdot 10^4$	$4 \cdot 10^{-5}$	$1 \cdot 10^5$	30
$M = 64$	100, 300, 300, 300, 240	169	100	120	64	$7 \cdot 10^3$	$8 \cdot 10^4$	$4 \cdot 10^{-5}$	$1 \cdot 10^5$	30

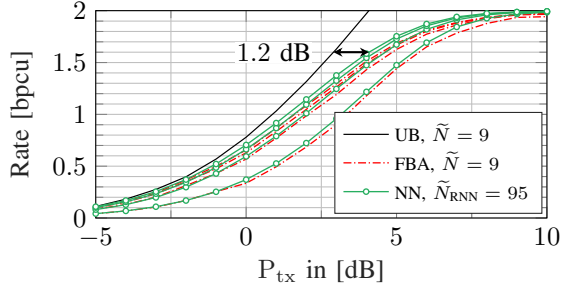


Fig. 5. 4-ASK, $L_{\text{fib}} = 30$ km. The rates increase with stages $S = 1, \dots, 4$; the lower curve of a certain style marks SDD; the upper curve marks $S = 4$.

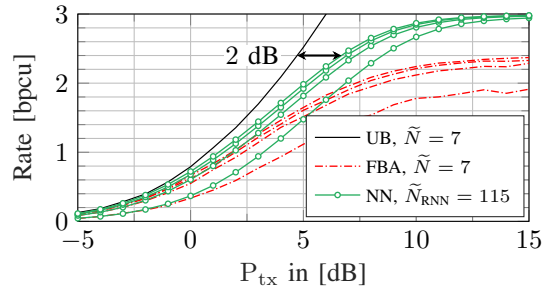


Fig. 6. 8-ASK, $L_{\text{fib}} = 30$ km. The rates increase with stages $S = 1, \dots, 4$; the lower curve of a certain style marks SDD; the upper curve marks $S = 4$.

number of multiplications per APP estimate. The FBA must use a mismatched channel memory $\tilde{N} \ll \tilde{K}$ because its complexity grows exponentially in \tilde{N} . The mismatched FBA memory is also much smaller than the NN memory. We compute the JDD upper bounds (UBs) of [42, Eq. (45)] via the mismatched FBA with the same memory \tilde{N} [19, Sec. III C].

Fig. 5 and Fig. 6 show the SIC rates via the FBA and NN for 4-ASK and 8-ASK, respectively. The rates increase with $S = 1, \dots, 4$. We run the FBA for 4-ASK and 8-ASK using $\tilde{N} = 9$ and $\tilde{N} = 7$ symbols, respectively. NN-SIC is at least as good as the mismatched FBA-SIC. For 8-ASK, the NN shows large gains over the FBA at medium to high SNRs because of the FBA channel mismatch. The NN substantially reduces the gap to the UB. Fig. 7 plots the rates of the NNs and bit-wise GS for 32-PAM/ASK and $S = 6$ stages. The FBA is infeasible for large constellations. GS runs with $N_{\text{par}} = 64$ samplers, $\tilde{N} = 21$ memory, and $N_{\text{iter}} = 125$ iterations. The performance of the NN and GS is similar at low SNRs. At high SNRs, GS stalls; see [48] and [6, Fig. 8]. The NN achieves the maximum rates for 32-PAM/ASK. Fig. 8 plots the rates for $S = 6$ and modulations up to $M = 64$. The gains over state-of-the-art unipolar PAM are ≈ 2.1 dB at 80% of the maximum rate. Fig. 9 visualizes the algorithmic complexity of Tab. I. For 32-PAM/ASK, the NN is 100 times less complex than GS.

VI. CONCLUSIONS

We designed time-varying RNN detectors for SIC and showed that they outperform FBA-SIC and GS-SIC with much less complexity. We simulated NN-SIC rates up to 6 bpcu with 64-PAM/ASK for a 30 km fiber-optic link with a SLD. Bipolar ASK gains up to ≈ 2.1 dB over state-of-the-art unipolar PAM.

ACKNOWLEDGMENT

The authors wish to thank M. Schädler, S. Calabrò, D. Lentner Ibanez and the reviewers for useful suggestions.

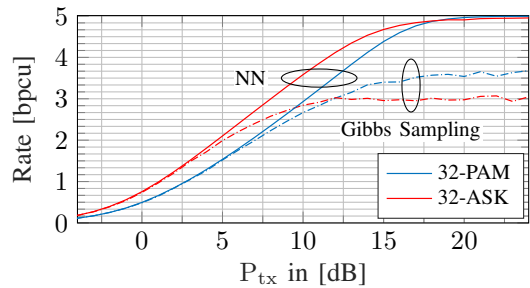


Fig. 7. $L_{\text{fib}} = 30$ km and $S = 6$. RNN: $\tilde{N}_{\text{RNN}} = 169$. Bit-wise GS [6]: $\tilde{N} = 21$, $N_{\text{iter}} = 125$ and $N_{\text{par}} = 64$.

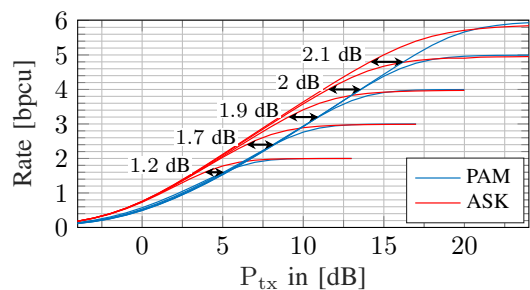


Fig. 8. NN-SIC rates for $L_{\text{fib}} = 30$ km, $S = 6$ and $M \in \{4, 8, 16, 32, 64\}$.

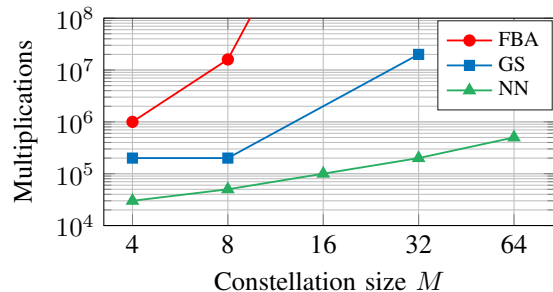


Fig. 9. Algorithmic complexity [20, Tab. IV].

REFERENCES

- [1] C. Mollén, *On massive MIMO base stations with low-end hardware*. Linköping University Electronic Press, 2016, vol. 1756.
- [2] M. Chagnon, "Optical communications for short reach," *J. Lightw. Technol.*, vol. 37, no. 8, pp. 1779–1797, April 2019.
- [3] R. Müller and W. Gerstacker, "On the capacity loss due to separation of detection and decoding," *IEEE Trans. Inf. Theory*, vol. 50, no. 8, pp. 1769–1778, 2004.
- [4] A. Sheikh, A. Graell i Amat, and G. Liva, "Achievable information rates for coded modulation with hard decision decoding for coherent fiber-optic systems," *J. Lightw. Technol.*, vol. 35, no. 23, pp. 5069–5078, 2017.
- [5] G. Liga, A. Alvarado, E. Agrell, and P. Bayvel, "Information rates of next-generation long-haul optical fiber systems using coded modulation," *J. Lightw. Technol.*, vol. 35, no. 1, pp. 113–123, 2017.
- [6] T. Prinz, D. Plabst, T. Wiegart, S. Calabrò, N. Hanik, and G. Kramer, "Successive interference cancellation for bandlimited channels with direct detection," *IEEE Trans. Commun.*, to appear.
- [7] C. Douillard, M. Jézéquel, C. Berrou, D. Electronique, A. Picart, P. Didier, and A. Glavieux, "Iterative correction of intersymbol interference: turbo-equalization," *Eur. Trans. Telecommun.*, vol. 6, no. 5, pp. 507–511, 1995.
- [8] P. D. Alexander, A. J. Grant, and M. C. Reed, "Iterative detection in code-division multiple-access with error control coding," *Eur. Trans. Telecommun.*, vol. 9, no. 5, pp. 419–425, 1998.
- [9] X. Wang and H. V. Poor, "Iterative (turbo) soft interference cancellation and decoding for coded CDMA," *IEEE Trans. Commun.*, vol. 47, no. 7, pp. 1046–1061, 1999.
- [10] U. Wachsmann, R. F. Fischer, and J. B. Huber, "Multilevel codes: Theoretical concepts and practical design rules," *IEEE Trans. Inf. Theory*, vol. 45, no. 5, pp. 1361–1391, 1999.
- [11] H. Pfister, J. Soriaga, and P. Siegel, "On the achievable information rates of finite state ISI channels," in *IEEE Global Telecommun. Conf.*, vol. 5, 2001, pp. 2992–2996 vol.5.
- [12] J. B. Soriaga, H. D. Pfister, and P. H. Siegel, "Determining and approaching achievable rates of binary intersymbol interference channels using multistage decoding," *IEEE Trans. Inf. Theory*, vol. 53, no. 4, pp. 1416–1429, 2007.
- [13] S. ten Brink, G. Kramer, and A. Ashikhmin, "Design of low-density parity-check codes for modulation and detection," *IEEE Trans. Commun.*, vol. 52, no. 4, pp. 670–678, 2004.
- [14] L. Bahl, J. Cocke, F. Jelinek, and J. Raviv, "Optimal decoding of linear codes for minimizing symbol error rate," *IEEE Trans. Inf. Theory*, vol. 20, no. 2, pp. 284–287, 1974.
- [15] J. Hagenauer and P. Hoeher, "A Viterbi algorithm with soft-decision outputs and its applications," in *IEEE Global Telecommun. Conf.*, 1989, pp. 1680–1686 vol.3.
- [16] D. J. C. MacKay, *Information Theory, Inference and Learning Algorithms*. Cambridge University Press, 2003.
- [17] J. Cioffi, G. Dudevoir, M. Vedat Eyuboglu, and G. Forney, "MMSE decision-feedback equalizers and coding. i. equalization results," *IEEE Trans. Commun.*, vol. 43, no. 10, pp. 2582–2594, 1995.
- [18] T. Koh and E. Powers, "Second-order Volterra filtering and its application to nonlinear system identification," *IEEE Trans. Acoustics, Speech, and Signal Proc.*, vol. 33, no. 6, pp. 1445–1455, 1985.
- [19] D. Plabst, T. Prinz, T. Wiegart, T. Rahman, N. Stojanović, S. Calabrò, N. Hanik, and G. Kramer, "Achievable rates for short-reach fiber-optic channels with direct detection," *J. Lightw. Technol.*, vol. 40, no. 12, pp. 3602–3613, 2022.
- [20] D. Plabst, T. Prinz, F. Diedolo, T. Wiegart, G. Böcherer, N. Hanik, and G. Kramer, "Neural network equalizers and successive interference cancellation for bandlimited channels with a nonlinearity," *submitted for publication in IEEE Trans. Commun.*, January 2024.
- [21] M.-H. Yang, J.-L. Chen, and P.-Y. Cheng, "Successive interference cancellation receiver with neural network compensation in the CDMA systems," in *Asilomar Conf. Sign., Syst., and Comp.*, vol. 2, 2000, pp. 1417–1420 vol.2.
- [22] C. Lin, Q. Chang, and X. Li, "A deep learning approach for MIMO-NOMA downlink signal detection," *Sensors*, vol. 19, no. 11, p. 2526, 2019.
- [23] J.-M. Kang, I.-M. Kim, and C.-J. Chun, "Deep learning-based MIMO-NOMA with imperfect SIC decoding," *IEEE Systems J.*, vol. 14, no. 3, pp. 3414–3417, 2020.
- [24] M. A. Aref and S. K. Jayaweera, "Deep learning-aided successive interference cancellation for MIMO-NOMA," in *IEEE Global Commun. Conf.*, 2020, pp. 1–5.
- [25] J. Kim, J. Kim, and M.-S. Lee, "Enhanced deep soft interference cancellation for multiuser symbol detection," *ETRI Journal*, 2023.
- [26] T. Van Luong, N. Shlezinger, C. Xu, T. M. Hoang, Y. C. Eldar, and L. Hanzo, "Deep learning based successive interference cancellation for the non-orthogonal downlink," *IEEE Trans. Vehic. Technol.*, vol. 71, no. 11, pp. 11 876–11 888, 2022.
- [27] T. M. Cover and J. A. Thomas, *Elements of Information Theory*, 2nd ed. John Wiley & Sons, Inc., Hoboken, NJ, USA, 2006.
- [28] H. Friis, "Noise figures of radio receivers," *Proc. IRE*, vol. 32, no. 7, pp. 419–422, 1944.
- [29] C. Rapp, "Effects of HPA-nonlinearity on a 4-DPSK/OFDM-signal for a digital sound broadcasting signal," *ESA Special Publication*, vol. 332, pp. 179–184, 1991.
- [30] A. Saleh, "Frequency-independent and frequency-dependent nonlinear models of TWT amplifiers," *IEEE Trans. Commun.*, vol. 29, no. 11, pp. 1715–1720, 1981.
- [31] D. Plabst, F. J. García-Gómez, T. Wiegart, and N. Hanik, "Wiener filter for short-reach fiber-optic links," *IEEE Commun. Lett.*, vol. 24, no. 11, pp. 2546–2550, 2020.
- [32] G. T. Zhou and R. Raich, "Spectral Analysis of Polynomial Nonlinearity with Applications to RF Power Amplifiers," *EURASIP J. Applied Signal Proc.*, vol. 2004, p. 256395, Dec. 2004.
- [33] G. Wise, A. Traganitis, and J. Thomas, "The effect of a memoryless nonlinearity on the spectrum of a random process," *IEEE Trans. Inf. Theory*, vol. 23, no. 1, pp. 84–89, 1977.
- [34] H. Ochiai, "An analysis of band-limited communication systems from amplifier efficiency and distortion perspective," *IEEE Trans. Commun.*, vol. 61, no. 4, pp. 1460–1472, 2013.
- [35] J. Huber, "Trelliscodierte digitale Übertragungsverfahren," in *Trelliscodierung*. Springer, 1992, pp. 141–260.
- [36] F. Schuh, A. Schenk, and J. B. Huber, "Reduced complexity super-trellis decoding for convolutionally encoded transmission over ISI-channels," in *Int. Conf. Comp., Netw., and Commun. (ICNC)*, 2013, pp. 484–489.
- [37] T. R. Giallorenzi and S. G. Wilson, "Multiuser ML sequence estimator for convolutionally coded asynchronous DS-SS-CDMA systems," *IEEE Trans. Commun.*, vol. 44, no. 8, pp. 997–1008, 1996.
- [38] H. Kim, S. Oh, and P. Viswanath, "Physical layer communication via deep learning," *IEEE J. Sel. Areas Inf. Theory*, vol. 1, no. 1, pp. 5–18, 2020.
- [39] S. Haykin, "Adaptive digital communication receivers," *IEEE Communications Magazine*, vol. 38, no. 12, pp. 106–114, 2000.
- [40] I. Goodfellow, Y. Bengio, and A. Courville, *Deep learning*. MIT press, 2016.
- [41] C. M. Bishop and N. M. Nasrabadi, *Pattern recognition and machine learning*. Springer, 2006, vol. 4, no. 4.
- [42] D. M. Arnold, H.-A. Loeliger, P. O. Vontobel, A. Kavčić, and W. Zeng, "Simulation-based computation of information rates for channels with memory," *IEEE Trans. Inf. Theory*, vol. 52, no. 8, pp. 3498–3508, 2006.
- [43] G. Böcherer, "Lecture notes on machine learning for communications," <http://www.georg-boecherer.de/mlcomm.pdf>, November 2021, [Online; accessed 20-April-2023].
- [44] D. P. Kingma and J. Ba, "Adam: A method for stochastic optimization," *arXiv preprint arXiv:1412.6980*, 2017.
- [45] R. Pascanu, T. Mikolov, and Y. Bengio, "On the difficulty of training recurrent neural networks," 2013.
- [46] P. Schniter and S. Rangan, "Compressive phase retrieval via generalized approximate message passing," *IEEE Trans. Sig. Proc.*, vol. 63, no. 4, pp. 1043–1055, 2015.
- [47] D. Plabst. (2024) NN-MI: Neural Network Achievable Information Rate Computation for Channels with Memory. [Online]. Available: <https://github.com/DPlabst/NN-MI>
- [48] M. Sens and G. Ascheid, "A Rao-Blackwellized Markov chain Monte Carlo algorithm for efficient MIMO detection," in *IEEE Int. Conf. Commun. (ICC)*. IEEE, 2011, pp. 1–6.